



## Article

# A Robust Control Scheme for Renewable-Based Distributed Generators Using Artificial Hydrocarbon Networks

Antonio Rosales <sup>1</sup> , Pedro Ponce <sup>1,\*</sup>, Hiram Ponce <sup>2</sup>  and Arturo Molina <sup>1</sup>

<sup>1</sup> School of Engineering and Sciences, Tecnológico de Monterrey, Campus Ciudad de México, Ciudad de México 14380, México; antonio.rosales@tec.mx (A.R.); armolina@tec.mx (A.M.)

<sup>2</sup> Facultad de Ingeniería, Universidad Panamericana, Ciudad de México 03920, México; hponce@up.edu.mx

\* Correspondence: pedro.ponce@tec.mx; Tel.: +52-55-5483-2165

Received: 8 February 2019; Accepted: 3 May 2019; Published: 18 May 2019



**Abstract:** Distributed generators (DGs) based on renewable energy systems such as wind turbines, solar panels, and storage systems, are key in transforming the current electric grid into a green and sustainable network. These DGs are called inverter-interfaced systems because they are integrated into the grid through power converters. However, inverter-interfaced systems lack inertia, deteriorating the stability of the grid as frequency and voltage oscillations emerge. Additionally, when DGs are connected to the grid, its robustness against unbalanced conditions must to be ensured. This paper presents a robust control scheme for power regulation in DGs, which includes inertia and operates under unbalanced conditions. The proposed scheme integrates a robust control algorithm to ensure power regulation, despite unbalanced voltages. The control algorithm is an artificial hydrocarbon network controller, which is a chemically-inspired technique, based on carbon networks, that provides stability, robustness, and accuracy. The robustness and stability of the proposed control scheme are tested using Lyapunov techniques. Simulation, considering one- and three-phase voltage sags, is executed to validate the performance of the control scheme.

**Keywords:** distributed generators; renewable energy; virtual synchronous generator; robust control; intelligent control

## 1. Introduction

Distributed generators (DGs) based on green-energy technologies are strongly promoted in governmental and industrial policies around in the world, due to agreements that promote the decrement of energy generation using fossil fuels [1,2]. Wind turbines, solar panels, and storage systems are the most promising technologies [3,4] to reduce the use of fossil fuels. Particularly, micro-grids are considered to be the key in future electric grids based on renewable energy, since a micro-grid groups DGs, storage systems, and loads in clusters to make the control and management of DGs easier [5]. DGs based on renewable energy resources are denominated inverter-interfaced units because a power converter is employed to tie the DG to the grid. As inverter-interfaced units, such as solar panels and storage systems, are non-synchronous generators, they lack rotational inertia, causing large frequency variations which affect the stability of the grid [6]. An useful alternative to alleviate instability is the addition of virtual inertia in the control scheme—namely, virtual synchronous generator (VSG) schemes—include artificial inertia in the control loop through the integration of a swing equation to emulate the rotational inertia of synchronous power generators [7].

DGs using the VSG scheme have been widely studied because they are capable to work in island and grid-connected modes [8]; however, their stability analysis and control design are studied under

balanced conditions. Additionally, DGs with VSG working in grid-connected mode are sensitive to grid disturbances, such as low voltage ride through (LVRT) and voltage sags [9,10]. Control schemes for DGs with virtual inertia dealing with unbalanced conditions are presented in [9–12], but the proposed control algorithms are linear proportional-integral-derivative (PID-type) algorithms, which present sensitivity to model variations [13,14].

Additionally, non-linear control techniques have been applied to DGs with the VSG scheme. In [15], a non-linear control algorithm was designed using a large signal model (non-linear), then the performance of VSG was tested with parameter variations; however, unbalanced conditions were not considered. Back-stepping control, as well as sliding mode control, were applied to VSG in [16]; despite the verified stability of the control scheme, the performance of the controller was only tested considering transitions from island to connected mode. Intelligent control techniques, such as neuronal networks and fuzzy logic control, were presented in [17,18], where the controllers were tested under disturbances (inertial variations), and different power commands, but unbalanced conditions were not verified. Therefore, robust control strategies for DGs based on renewable energy technologies are required: They must be capable of addressing lack of inertia and sensitivity against parameter variations, as well as unbalanced conditions.

Fuzzy logic control (FLC) can address the problem of model variations, as its design does not require the use of mathematical models; it transforms human knowledge into a non-linear mapping [19], which defines the control input to be applied, in accordance to defined if-then rules. Naturally-inspired computing has been applied to improve the performance of FLC systems by means of the use of meta-heuristic optimization methods, social communication techniques, chemical structure-based learning algorithms, and so on [20]. Particularly, artificial hydrocarbon networks (AHN) provide a useful computational algorithm for control and modeling problems [21]. Stability, robustness, and accuracy are the main characteristics of AHN [21] because it is a chemically inspired technique, based on carbon networks, which catches stability in the topology of the algorithm and partial knowledge of the system behavior [20]. Thus, control algorithms with AHN are capable of dealing with uncertain, imprecise, and noisy data [22]. The efficacy of AHN control systems is supported by its application in a position controller of the two-axes tool in a computer numerical control (CNC) for high-precision machines [23], a liquid-level controller in a coupled-tanks system [24], and a controller for a doubly-fed induction generator wind turbine [22], among others.

In this paper, a robust control scheme for DGs operating under unbalanced conditions is proposed. The presented scheme is composed of an AHN controller to regulate reactive power while an active power loop maintains the conventional topology of the VSG to preserve inertia. Thus, the contributions of this paper can be summarized as:

- A robust control scheme capable of regulating reactive power, where inertia is included through the VSG scheme to preserve stability; and
- A control scheme able to accomplish robust power regulation, as it works under voltage-unbalanced conditions, which is the main drawback of DGs with VSG. Furthermore, the robustness is preserved during changes from connected to island mode, and vice versa.

The properties of the control scheme based on AHN are validated by simulations considering one- and three-phase voltage sags.

The structure of the paper is as follows: The control scheme is presented in Section 2; the bases of AHN are given in Section 3; the proposed robust control scheme is proposed in Section 4; and the simulations are shown in Section 5.

## 2. Problem Statement

Consider the control scheme presented in Figure 1, which is widely employed to include virtual inertia in DGs [7]. Reactive  $Q$  and active  $P$  power control loops are part of the scheme, both in a  $dq$  reference frame. The  $P$  loop contains the following elements [25]. The active power calculation,

$$P_{out} = v_d i_d + v_q i_q, \quad (1)$$

where  $i_d$ ,  $i_q$ ,  $v_d$ , and  $v_q$  are the currents and voltages in the inverter terminal on a  $dq$  rotating reference frame. Then,  $v_{dq}$  and  $i_{dq}$  are computed as

$$h_{dq} = \begin{bmatrix} h_d \\ h_q \\ h_0 \end{bmatrix} = \frac{2}{3} \begin{bmatrix} 1 & \cos(-\frac{2\pi}{3}) & \cos(\frac{2\pi}{3}) \\ 0 & -\sin(-\frac{2\pi}{3}) & -\sin(\frac{2\pi}{3}) \\ \frac{1}{2} & \frac{1}{2} & \frac{1}{2} \end{bmatrix} \begin{bmatrix} h_a \\ h_b \\ h_c \end{bmatrix}, \quad (2)$$

where  $h_{dq}$  represents  $v_{dq}$  or  $i_{dq}$ .

The rotor swing equation

$$J\omega_m \frac{d\omega_m}{dt} = P_{in} - P_{out}, \quad (3)$$

where  $\omega_m$  is the virtual rotor angular frequency,  $J$  the inertia, and the block named governor represents a droop characteristic, defined as in [6],

$$P_{in} = P_0 + m_p(\omega_0 - \omega_m), \quad (4)$$

where  $\omega_0$  is the nominal angular frequency,  $m_p$  is the droop coefficient, and  $P_0$  is a given set active power.

On the other hand, the  $Q$  loop contains the next elements [25]. The reactive power calculation block consists of

$$Q_{out} = v_d i_q - v_q i_d. \quad (5)$$

The voltage droop block generates the reference of reactive power  $Q_{out}^*$ , and is computed as

$$Q_{out}^* = Q_0 + m_q(V_0 - V_t), \quad (6)$$

where  $Q_0$  is given set reactive power,  $V_0$  is a reference of voltage,  $m_q$  is the droop coefficient, and  $V_t$  is the voltage rms of the filter output. The reactive power controller is

$$E = G_{PI}(Q_{out}^* - Q_{out}) + V_0, \quad (7)$$

where  $G_{PI}$  is the transfer function of a proportional-integral (PI) controller.

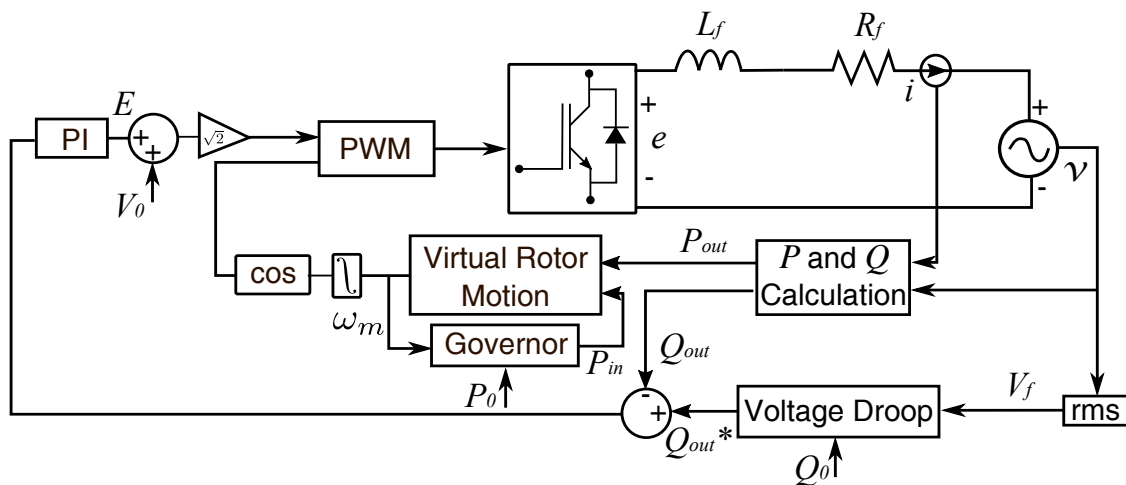


Figure 1. Control scheme for distributed generators (DGs) including virtual inertia.

The relation between inverter output current, terminal voltage, and inverter side voltage is represented by the dynamics of the filter inductor [26],

$$\begin{bmatrix} \dot{i}_d \\ \dot{i}_q \end{bmatrix} = \begin{bmatrix} -\frac{R_f}{L_f} & \omega_0 \\ -\omega_0 & -\frac{R_f}{L_f} \end{bmatrix} \begin{bmatrix} i_d \\ i_q \end{bmatrix} + \begin{bmatrix} \frac{1}{L_f} & 0 \\ 0 & \frac{1}{L_f} \end{bmatrix} \begin{bmatrix} e_d - v_d \\ e_q - v_q \end{bmatrix}, \quad (8)$$

where  $i_d$ ,  $i_q$ ,  $v_d$ , and  $v_q$  are the currents and voltages in the inverter terminal,  $e_d$  and  $e_q$  are the inverter side voltages,  $\omega_0$  is nominal frequency (generator), and  $L_f$  and  $R_f$  are inductance and resistance of filter's inductor.

Taking into account the equations of the control scheme in Figure 1 ((1)–(8)), one can note the following issues:

- The dynamics in Equation (8) do not consider unbalanced conditions (i.e., the grid voltage is balanced and no negative sequence components are integrated). So, any study employing Equation (8) can not describe the practical conditions of DGs connected to the grid.
- Reactive power is regulated using conventional PI controllers, which presents sensitivity to model variations and disturbances such as unbalanced voltage conditions.

This paper proposes a robust control algorithm to tackle the aforementioned issues. The proposed scheme is capable of compensating for model variations and disturbances due to unbalanced conditions while inertia is maintained.

In the next section, the basis of AHN is presented to understand the robust control algorithm given later.

### 3. Artificial Hydrocarbon Networks

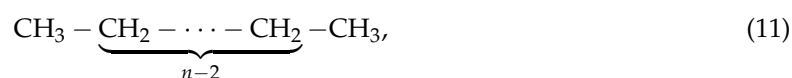
An artificial hydrocarbon network (AHN) is a supervised learning method capable of extracting information from and to model data, which is inspired by chemical hydrocarbon compounds [21]. The basic units of AHN are carbon and hydrogen molecules (CH-molecules), and each CH-molecule produces an output response  $\varphi$  associated to an input  $x$  [20],

$$\varphi(x) = \rho \prod_{i=1}^{k \leq 4} (x - h_i), \quad (9)$$

where  $\rho \in \mathbb{R}$  is the carbon value,  $h_i \in \mathbb{C}$  are the hydrogen values (i.e., hydrogen atoms attached to the carbon atom), and  $k$  is the degree of freedom in the molecule. Two or more CH-molecules can be grouped to form an AHN-component, named an artificial hydrocarbon compound, which is described as follows,

$$\psi(\varphi_1, \dots, \varphi_n, x) = \begin{cases} \varphi_1(x) & L_0 \leq x < L_1; \\ \vdots & \\ \varphi_n(x) & L_{n-1} \leq x \leq L_n, \end{cases} \quad (10)$$

where  $\psi$  is the behavior of the compound,  $\varphi_n(x)$  are the molecular behaviors, and  $L_n$  are the bounds of the molecules (i.e., the limits of the output response of each molecule produced by input  $x$ ). A particular structural representation of an artificial hydrocarbon compound is



where  $n$  is the number CH-molecules (i.e., molecular behaviors). Details about an optimal algorithm to compute the distance between molecules was presented in [20]. Thus, an AHN is a combination of artificial hydrocarbon compounds useful to predict, to model, and to classify data based on chemical rules [22].

### 3.1. Fuzzy-Molecular Interface Systems

The block diagram in Figure 2 describes a fuzzy-molecular interface system, which consists of three steps [21]: Fuzzification, the fuzzy inference engine, and molecular de-fuzzification (i.e., a de-fuzzification process using AHN). Fuzzification consists of mapping the input  $x$  to a fuzzy value  $[0, 1]$  by means of a fuzzy set and its membership function,

$$\mu_A : x \rightarrow [0, 1]. \quad (12)$$

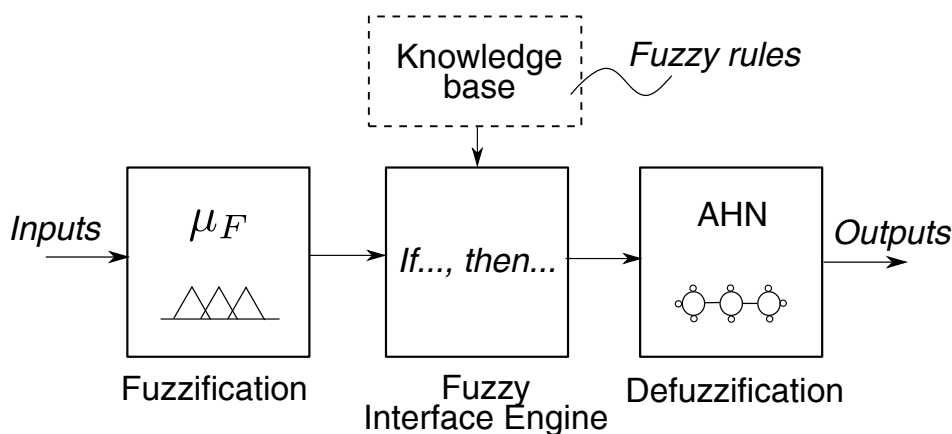


Figure 2. Block diagram of fuzzy-molecular interface systems.

The fuzzy inference engine consists of the evaluation of antecedents in terms of fuzzy rules:

$$R_i : \text{If } \Delta(x_1 \text{ is } A_1, \dots, x_k \text{ is } A_k), \text{ then } y_i = \varphi_j(\mu_\Delta(x_1, \dots, x_k)), \quad (13)$$

where  $\varphi_j$  is the molecular behavior of the  $j$ th CH-molecule ( $M_j$ ) of the AHN, and  $\mu_\Delta(x_1, \dots, x_k)$  is computed as

$$\mu_\Delta(x_1, \dots, x_k) = \min\{\mu_{A_1}(x_1), \dots, \mu_{A_k}(x_k)\}.$$

Then, the consequent value  $y_i$  is obtained as

$$y_i = \varphi_j(\min\{\mu_{A_1}(x_1), \dots, \mu_{A_k}(x_k)\}). \quad (14)$$

Finally, in the defuzzification stage, the crisp value of  $y$  is computed as

$$y = \frac{\sum \mu_{\Delta_i}(x_1, \dots, x_k) \cdot y_i}{\sum \mu_{\Delta}(x_1, \dots, x_k)}. \quad (15)$$

The knowledge base is a matrix that summarizes the fuzzy rules presented in (13), considering the combination of all input variables  $x_1, \dots, x_k$ , and the molecules  $M_j$ . Assuming the rules

$$\begin{aligned} R_1 : & \text{If } x_1 \text{ is } A_1 \text{ and } x_2 \text{ is } B_2, \text{ then } y_1 \text{ is } M_1 \\ R_2 : & \text{If } x_1 \text{ is } A_2 \text{ and } x_2 \text{ is } B_1, \text{ then } y_2 \text{ is } M_1, \\ R_3 : & \text{If } x_1 \text{ is } A_1 \text{ and } x_2 \text{ is } B_1, \text{ then } y_3 \text{ is } M_2 \end{aligned} \quad (16)$$

an example of this matrix is presented in Table 1.

The advantages of the fuzzy model interface are [21]: The fuzzy partitions in the output domain might be seen as linguistic units (for example, “low” and “high”); fuzzy partitions have a degree of understanding (the parameters are metadata); and molecular units deal with noise and uncertainties.

**Table 1.** Knowledge base example for Equation (16).

$x_1$	$x_2$	$y_1$
$A_1$	$B_2$	$M_1$
$A_2$	$B_1$	$M_1$
$A_1$	$B_1$	$M_2$

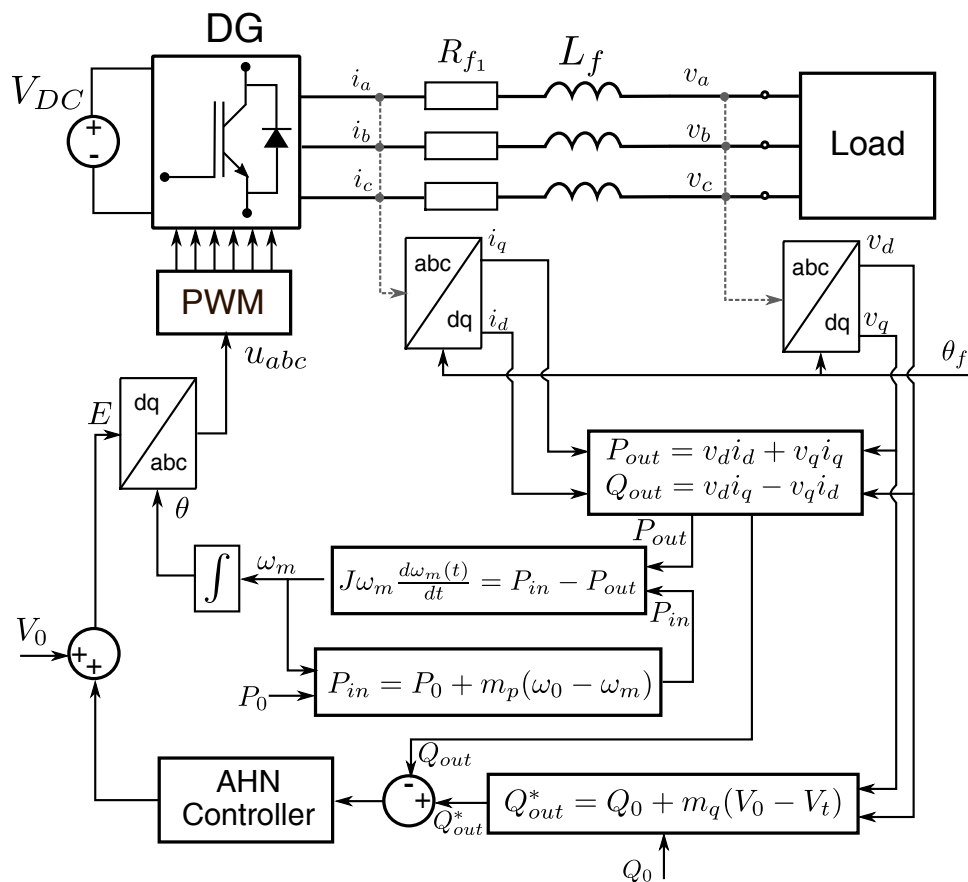
### 3.2. AHN Controller

A control algorithm that executes its control effort using a fuzzy-molecular interface system is known as AHN controller [22], which is able to deal with uncertain and noisy data. Moreover, the design of AHN controllers is easy, because CH-molecules integrate expert and real-data information in single units.

The detailed control scheme for DG using an AHN controller is presented in the next section.

## 4. Robust Control Scheme Using AHN

Figure 3 presents the diagram of the proposed robust control scheme, where two control loops can be identified: The first one, related to the active power  $P$  regulation ( $P$ -loop) and the second one with reactive power  $Q$  regulation ( $Q$ -loop).  $P$  and  $Q$  are computed using the  $dq$  components with angular position  $\theta_f = \omega t$ , where  $\omega$  is the rotational frequency of the  $dq$  frame. The  $P$ -loop contains the virtual inertia necessary to suppress frequency oscillations, which is preserved as in the conventional VSG scheme. The  $Q$ -loop integrates an AHN controller, instead of the conventional PI control (see Figure 1), to provide a robust regulation of reactive power. In this section, the design of the robust AHN controller is presented.

**Figure 3.** Diagram of the robust control scheme using an artificial hydrocarbon network (AHN).

The proposed AHN controller is composed of a fuzzy sliding surface in a feedback loop with a fuzzy-molecular interface system, see Figure 4.

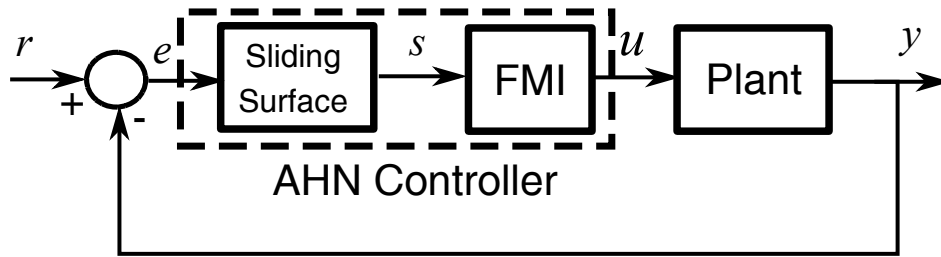


Figure 4. Block diagram of the AHN controller.

The fuzzy sliding surface is defined as

$$s = \int e + \lambda e, \quad (17)$$

where  $\lambda > 0$  is a constant and  $e$  is the regulation error. The state-space representation of  $s$  is shown in Figure 5 [27]. Thus, the AHN controller does not response to changes in the regulation error  $e$  or its derivatives, but it reacts to changes in  $s$ ; therefore, the number of fuzzy rules is reduced compared with classical fuzzy logic control.

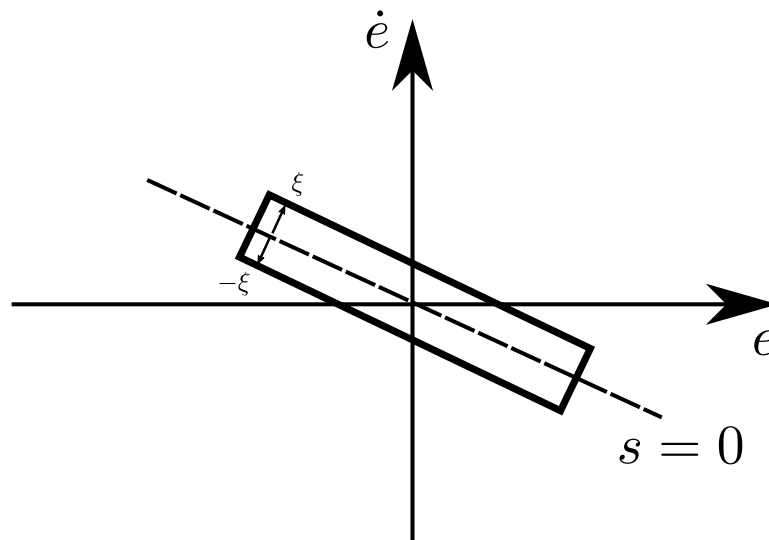


Figure 5. Fuzzy sliding surface.

The rules to be implemented in the fuzzy-molecular interface of the AHN controller are as follows:

- $R_1$  : If  $s$  is NB then  $u$  is Bigger
  - $R_2$  : If  $s$  is NM then  $u$  is Big
  - $R_3$  : If  $s$  is ZR then  $u$  is Medium
  - $R_4$  : If  $s$  is PM then  $u$  is Small
  - $R_5$  : If  $s$  is PB then  $u$  is Smaller,
- (18)

where NB, NM, ZR, PM, and PB mean negative big, negative medium, zero, positive medium, and positive big, respectively. Note that the objective of the fuzzy-molecular interface is to keep  $s \approx 0$ ; thus, if  $s = \int e + \lambda e \approx 0$ , the dynamics of the system driven by the AHN controller is reduced to

$\dot{e} = -\lambda e$ , which has a solution  $e(t) = e^{-\lambda t}$ . Therefore, when  $s \approx 0$ , the regulation error  $e$  converges asymptotically to zero, and does not depend on the parameter of the system to be controlled.

The output of the fuzzy-molecular interface results in the control input presented in Figure 6, which can be represented as [27]

$$u = -M \cdot \text{sigm}\left(\frac{s}{\Phi}\right), \quad (19)$$

where  $M$  is the maximum value of the control gain and  $\text{sigm}$  is the sigmoid function, defined by

$$\text{sigm}(s) = \begin{cases} -1 & s < -1; \\ -\frac{1}{2} \frac{(2s+3)(3s+1)}{4s^2+6s+1} & -1 \leq s < -\frac{1}{2}; \\ -\frac{1}{2} \frac{s(2s+3)}{4s^2+2s-1} & -\frac{1}{2} \leq s < 0; \\ \frac{1}{2} \frac{s(2s-3)}{4s^2-2s-1} & 0 \leq s < \frac{1}{2}; \\ \frac{1}{2} \frac{(2s-3)(3s-1)}{4s^2-6s+1} & \frac{1}{2} \leq s < 1; \\ 1 & s \geq 1. \end{cases} \quad (20)$$

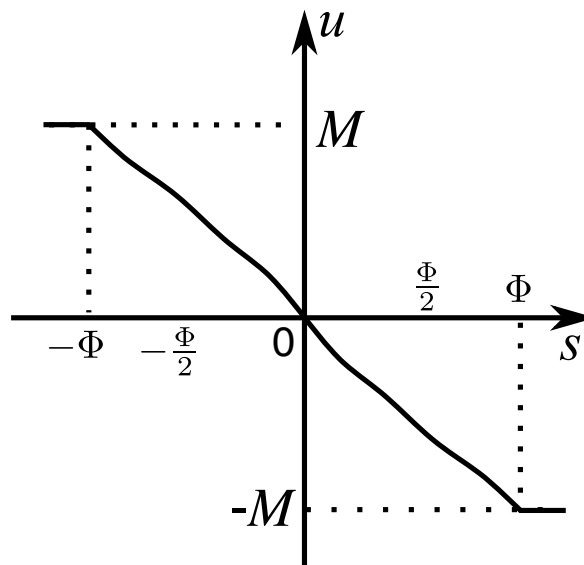


Figure 6. Output of the AHN controller with sliding surface.

Note that function (20) is similar to the AHN-component in Equation (10), then a CH-molecular representation can be obtained, as in Equation (11). Moreover, the form of AHN control is similar to a saturation function. The computation of gain  $M$  and the test of stability of the AHN controller are presented in the next subsection.

#### 4.1. Design of AHN Controller for DG

Define the tracking error of reactive power  $Q$  as

$$e_q = Q_{out} - Q_r, \quad (21)$$

where  $Q_r$  is the reactive power reference and  $Q_{out}$  is the reactive power measured from inverter output. Consider the Lyapunov function [28]

$$V(x) = \frac{1}{2}s^2, \quad (22)$$



where  $s = \int e + \lambda e$ , and whose derivative,  $\dot{V}$ , is

$$\dot{V}(x) = s\dot{s} = s [Q_{out} - Q_r + \lambda (\dot{Q}_{out} - \dot{Q}_r)] . \quad (23)$$

Assuming balance conditions and  $Q_r$  constant, the reactive power is defined by Equation (5) and  $\dot{Q}_r = 0$ , then

$$\dot{V}(x) = s [e + \lambda (-v_q i_d - i_d v_q + v_d i_q + v_d i_q)] . \quad (24)$$

Adding Equation (8) into Equation (24), and assuming the derivatives  $\dot{v}_d = \dot{v}_q = 0$  (since the inverter output voltages  $v_d, v_q$  are constants, see Equation (2)), we obtain

$$\dot{V}(x) = s \left[ e + \lambda \left( \frac{R_f}{L_f} Q_{out} + \frac{1}{L_f} [v_q e_d - v_d e_q] + \omega_0 P \right) \right] = s \left[ e + \lambda \left( \frac{R_f}{L_f} Q_{out} + g u + \omega_0 P \right) \right] , \quad (25)$$

where  $\omega_0$  is the nominal angular frequency,  $g = (v_q \cos \theta - v_d \sin \theta) / L_f$ , and  $u$  is the control input to be designed. Defining  $u = (\lambda g)^{-1} [-e - \lambda \frac{R_f}{L_f} Q_{out} - v]$  and replacing it in Equation (25), one gets

$$\dot{V}(x) = \sigma [-v + \psi(t)] , \quad (26)$$

where  $\psi = \omega_0 P$  is the disturbance term. Choosing  $v = M \text{sign}(s)$  with  $M > 0$ , and considering  $\psi < D$ ,  $\dot{V}$  is rewritten as

$$\dot{V}(x) = -s [M \text{sign}(s) - \psi(t)] < -|s| [M - D] . \quad (27)$$

Therefore, selecting  $M > D$  ensures that the trajectories converge to  $\sigma = 0$ , despite the presence of a disturbance  $\psi$ , and the tracking error  $e$  is asymptotically stable.

#### 4.2. Design for Unbalanced Conditions

Negative sequence components emerge in the DG scheme when the grid voltage is unbalanced. The reactive power under unbalanced conditions is computed as [11,29],

$$Q = v_q^+ i_d^+ - v_d^+ i_q^+ + v_q^- i_d^- - v_d^- i_q^- , \quad (28)$$

where  $+$  and  $-$  represent the voltage/currents of positive and negative sequences, respectively. Note that the zero sequence components are not studied in Equation (28), which does not represent a weakness for application since three-phase, three-wire unbalanced systems require the use of a negative sequence.

Including Equation (28) into Equation (25), the derivative,  $\dot{V}$ , is

$$\dot{V}(x) = s \left[ e + \lambda \left( \frac{R_f}{L_f} (Q_{out}^+ + Q_{out}^-) + g u + \omega_0 (P_{out}^+ + P_{out}^-) + \psi_d \right) \right] , \quad (29)$$

where  $Q_{out}^-$  and  $P_{out}^-$  are the negative sequence reactive and active power, respectively; and the disturbance term is  $\psi_d = v_q^+ i_q^+ - v_d^+ i_q^+ - v_q^- i_q^- - v_d^- i_q^-$ . Then, the derivative of  $V$ , considering the perturbed dynamics for reactive  $Q_{out}$ , can be rewritten as

$$\dot{V}(x) = s \left[ e + \lambda \left( \frac{R_f}{L_f} Q_{out}^+ + g u + \xi \right) \right] , \quad (30)$$

where  $\xi < D_d$  is a disturbance composed of the unbalance voltage terms (i.e., sequence negative components), as well as active power terms. Then, choosing  $u = (\lambda g)^{-1} [-e - \lambda \frac{R_f}{L_f} Q_{out}^+ - v]$  with  $v = M \text{sign}(s)$ , the gain  $M$  must be selected as  $M > D_d$ , where  $D_d$  is the upper bound of disturbance  $\xi$ .

Note that parameter variations, such as  $\Delta R_f, \Delta L_f$ , can be included in the disturbance term  $\xi$ ; therefore, the selection of a control gain  $M > D_d$  also ensures robustness against parameter variations.

As the term  $v = M \text{sign}(s)$  is a discontinuous term, which causes high frequency oscillations in the control system, the function sign is replaced by the sigmoid function defined by Equation (20) and Figure 6. As has been validated in [27,28], the controller  $u = (\lambda g)^{-1} \left[ -e - \lambda \frac{R_f}{L_f} Q_{out}^+ - v \right]$  with a sigmoid function, as in Figure 6, is a boundary-layer controller, which presents the robustness verified by the Lyapunov analysis using the function in Equation (22).

Therefore, the design of the proposed AHN controller consists of the following steps:

1. Define the fuzzy sliding variable as  $s = \int e + \lambda e$ ;
2. Design the fuzzy-molecular interface in Figure 2 with the rules in (18);
3. Select the value of  $M$  using the inequality  $M > D_d$  to compensate disturbances contained in  $\xi$ ; and
4. Implement the control law  $u = (\lambda g)^{-1} \left[ -e - \lambda \frac{R_f}{L_f} Q_{out}^+ - v \right]$  with  $v = M \text{sign}(s)$ .

Note that the design of the AHN controller has the following advantages: Employing less membership functions, since the rules are defined with respect to the fuzzy sliding surface instead of the error and its derivatives (as in conventional fuzzy logic control); and robustness against bounded coupled disturbances, because  $M$  considers the disturbed system.

## 5. Simulation Results

In order to validate the proposed control scheme, the circuit presented in Figure 7 is implemented in Matlab-Simulink (2018a, MathWorks, Natick, MA, USA), where the block named DG (Distributed Generator) contains the scheme of Figure 3, which regulates the controller voltage source (VS), and the parameters of the  $RL$  filter and loads. The parameters of the VSG Equations (1)–(6) are as follows:  $m_p = 48873$ ,  $m_q = 1250$ , and  $J = 28$ . Figure 8 shows the Simulink blocks used for the simulation.

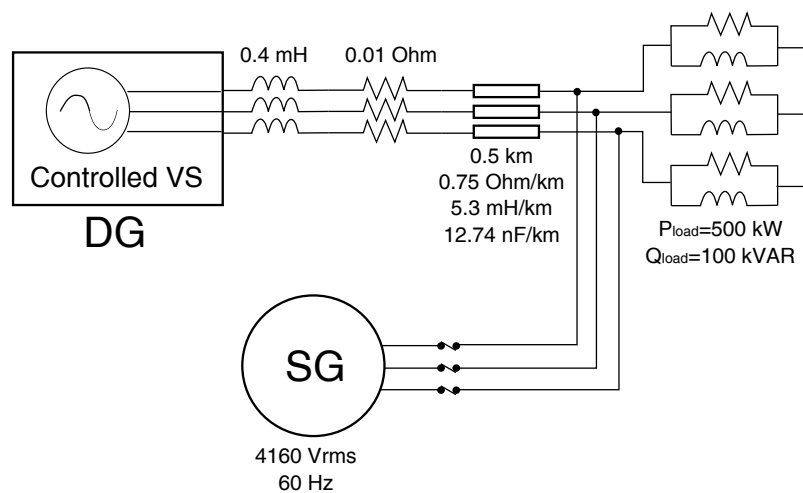


Figure 7. Simulation Circuit.

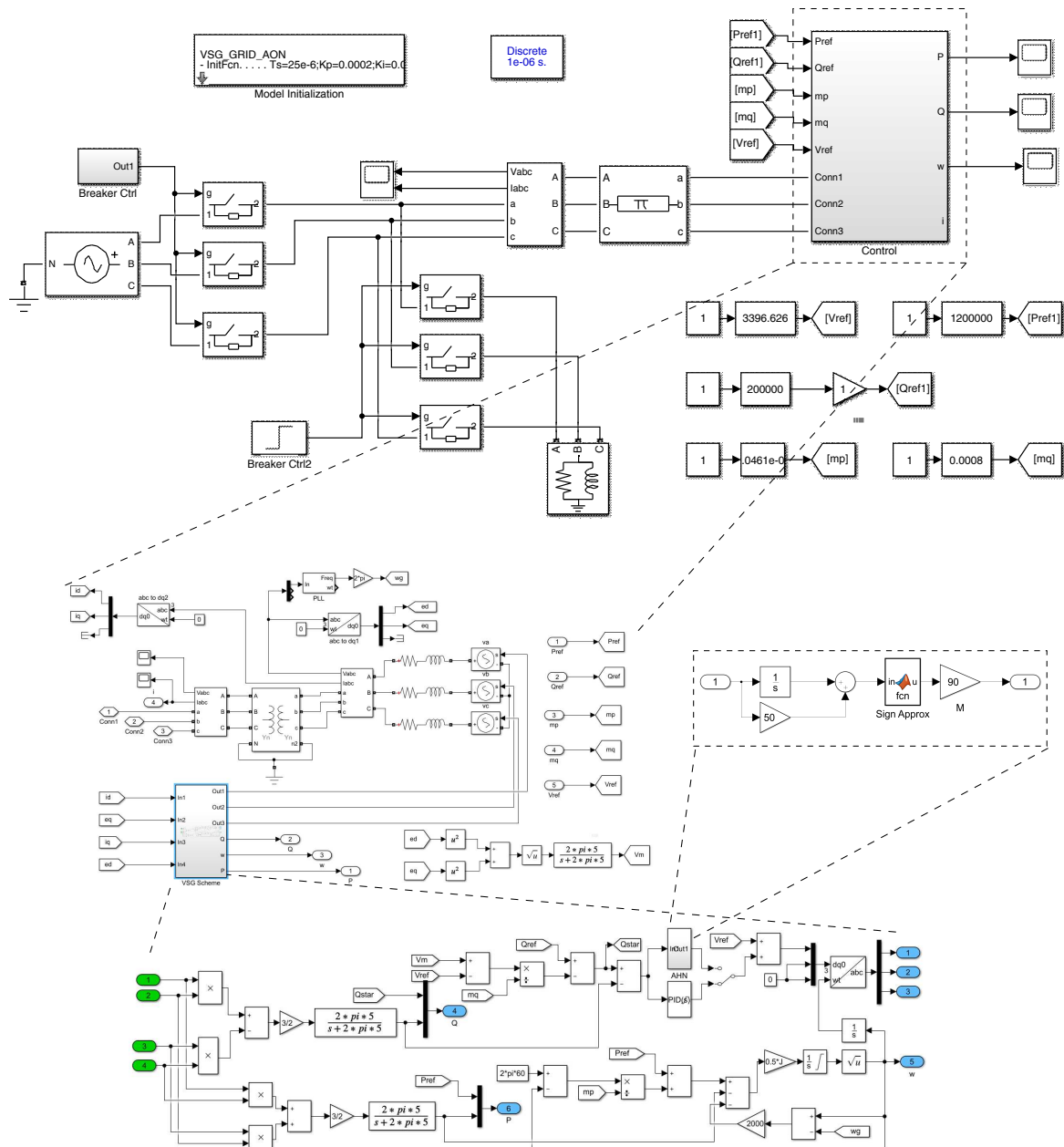


Figure 8. Block diagram implemented in Simulink.

The fuzzy sliding variable is selected as  $s = \int e + 50e$ . The designed fuzzy-molecular interface is the following:

$$\psi = \begin{cases} 1.3070(x - 0.9824 - i0.7844)(x - 0.9824 + i0.7844)(x + 0.4028); & 0.2 \leq x < 0.7; \\ -27.4971(x - 0.3731)(x + 0.0007); & 0 \leq x < 0.2; \\ 27.4971(x + 0.3731)(x - 0.0007); & -0.2 \leq x < 0; \\ 1.3070(x + 0.9824 - i0.7844)(x + 0.9824 + i0.7844)(x - 0.4028); & -0.7 < x < -0.2, \end{cases}$$

which has the structure presented in Figure 9, and has control gain  $M = 100$ . The membership functions of the AHN are presented in Figure 10.

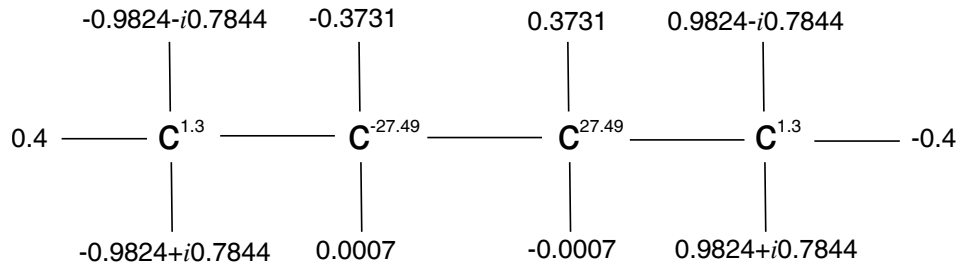


Figure 9. Artificial hydrocarbon network structure.

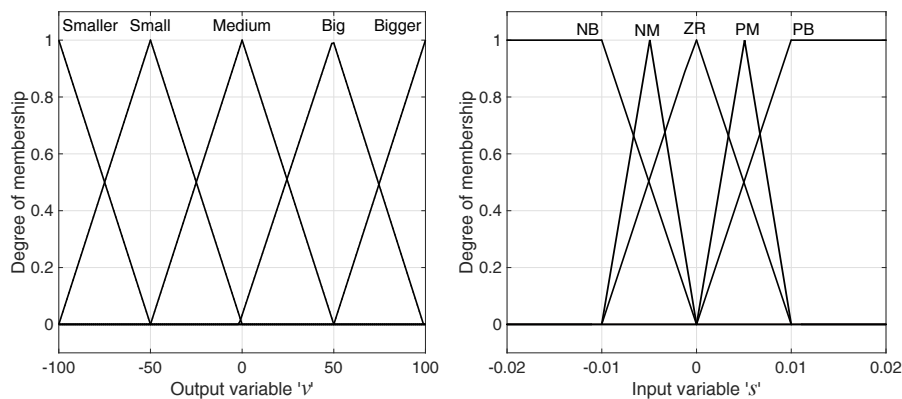
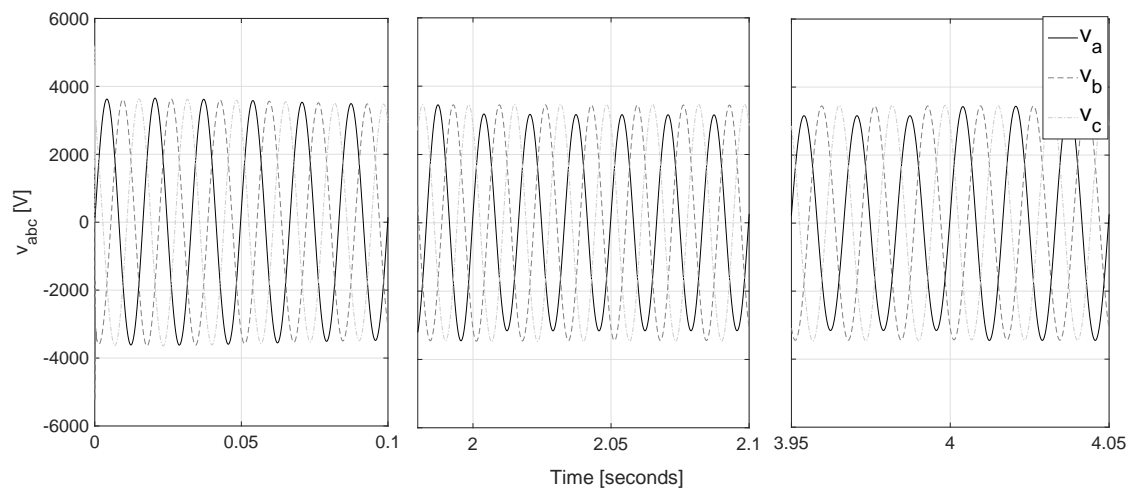


Figure 10. Membership functions of the AHN.

The simulation conditions are the following: Simulation time is 5 s; fixed step size of 1  $\mu$ s; and the solver is ode1 (Euler). The unbalance voltage conditions are emulated by means of voltage sags (i.e., a decrement in the voltage amplitude of the synchronous generator). All the analyzed voltage sags are decremented from 1 p.u to 0.9 p.u in the voltage amplitude. In order to compare the performance of the proposed control scheme, a PI controller, with gains  $K_i = 0.009$  and  $K_p = 1.5 \times 10^{-4}$ , is also implemented. The PI gains are tuned considering the same reach time, from initial conditions to reactive power reference, as the AHN controller.

Three simulation tests are presented considering  $P_0 = 1.2$  MW,  $Q_0 = 200$  kVAr, and the parameters of the circuit of Figure 7. The control objective is to regulate active and reactive power at  $P_0 = 1.2$  MW and reference  $Q_{out}^*$  in Equation (6). The first test considers a voltage sag, in phase 'a', at time  $t = 2$  s, which is maintained until  $t = 4$  s; the second test is executed under same conditions as test one, but the voltage sag is applied in the three phases, 'a', 'b', and 'c'; and the third test presents the transition between grid-connected and island modes, where  $t = 1$ –3 s is grid-connected mode, and island mode is maintained from  $t = 3$ –4 s. Finally, at  $t = 4$  s, grid-connected mode is activated again.

The voltages  $a, b, c$  for Tests 1 and 2 are presented in Figures 11–14, respectively. The voltages sag at 2 s and where it is removed at 4 s can be observed.



**Figure 11.** Simulation of voltages  $v_{abc}$  during Test 1, with PI control.

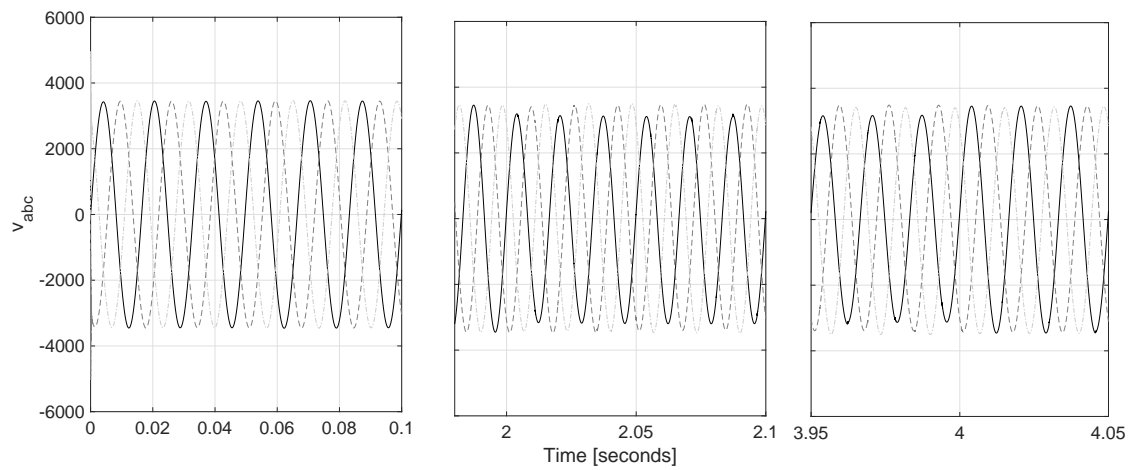


**Figure 12.** Simulation of voltages  $v_{abc}$  during Test 1, with PI and AHN controls.

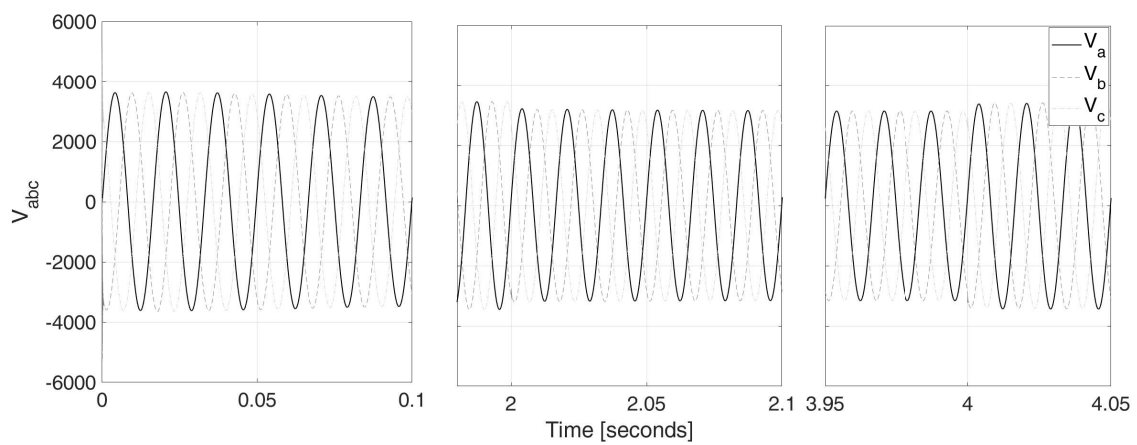


**Figure 13.** Simulation of voltages  $v_{abc}$  during Test 2, with PI control.

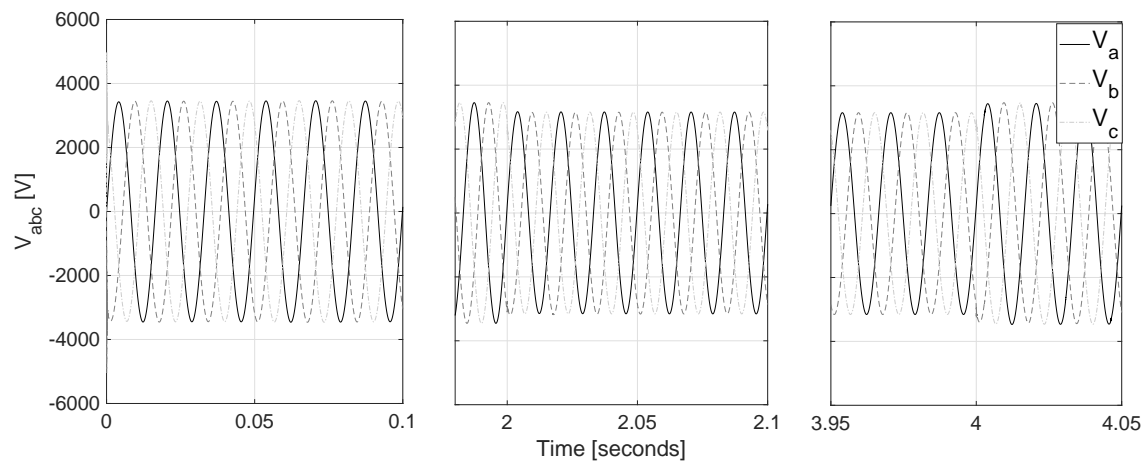


Figure 14. Simulation of voltages  $v_{abc}$  during Test 2, with AHN control.

The simulation results of Test 1 are presented in Figure 15, for the system with the AHN controller and PI. Reactive regulation is accomplished with both controllers, despite the effect of the voltage sag at  $t = 2$  s. However, the transient response of the system with PI presents a overshoot five times bigger than the system with AHN controller.

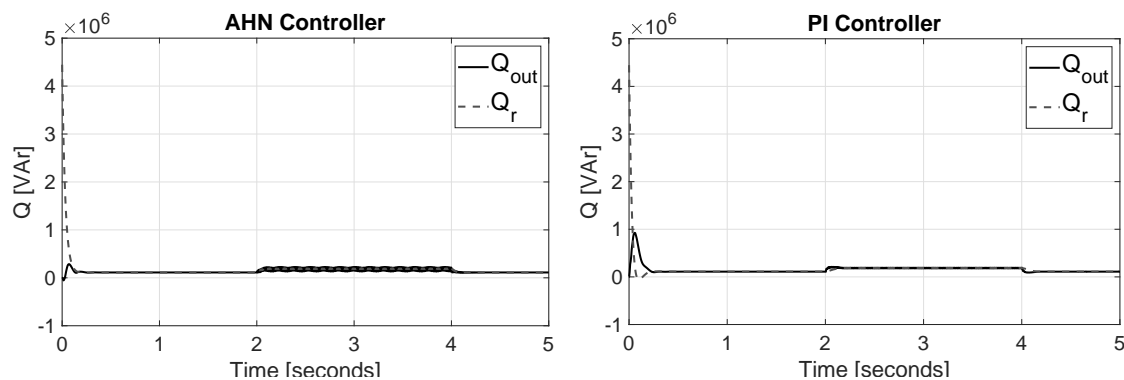


Figure 15. Simulation of reactive power regulation in Test 1.

For Test 2, the results are presented in Figure 16. Voltage sag emerges in the three phases at  $t = 2$  s, where it can be seen that (similar to the one-phase sag test) the proposed AHN controller ensures reactive power regulation with a lesser overshoot than PI control.

Test 3, with a transition between grid-connected and island modes and vice versa, is presented in Figure 17. One can observe that the transient response with AHN controller is still better than PI, since the overshoot is minor.

The regulation error,  $e_q$ , for Tests 1–3, are presented in Figures 18–20, respectively. One can observe that, during the changes resulting from the transition (0.5–1 s) and the voltage sags, the proposed AHN controller maintained a regulation error closer to zero, when compared with the PI controller. When the voltage sag appeared (disappeared) at 2 s (4 s), the PI control was not capable of regulating the reactive power in the reference, and  $e_q$  moved away from zero; see Figures 18 and 19. Additionally, when the DG was reconnected to the grid during Test 3 (see Figure 20), the system with PI control could not maintain the error closer to zero as the AHN control did. Thus, the proposed AHN is robust to voltage sags.

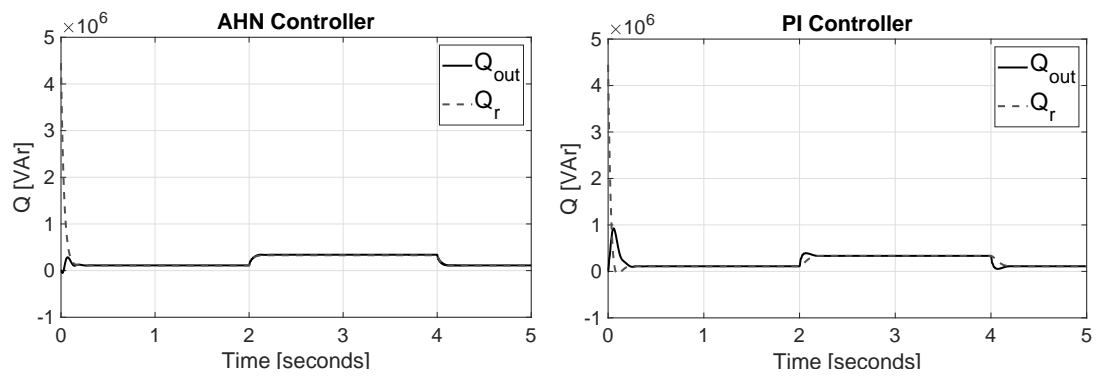


Figure 16. Simulation of reactive power regulation: Test 2.

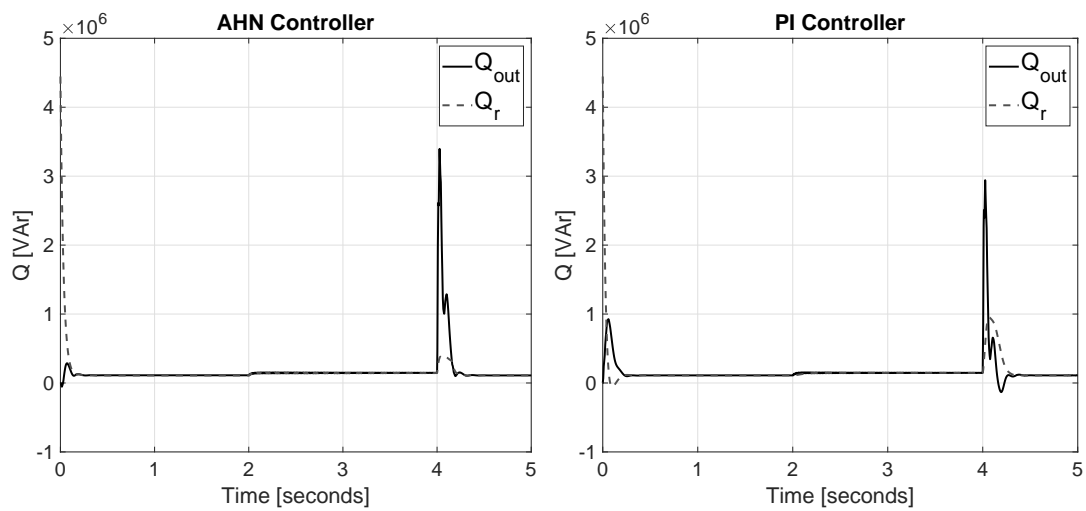


Figure 17. Simulation of reactive power regulation: Test 3.

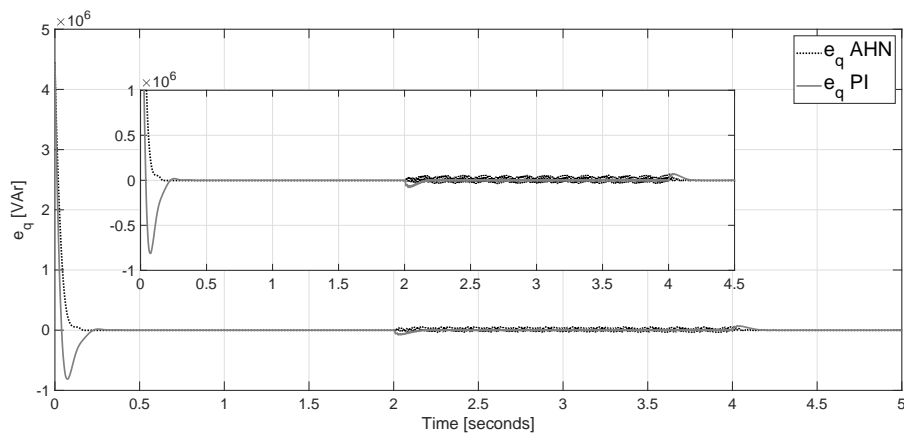
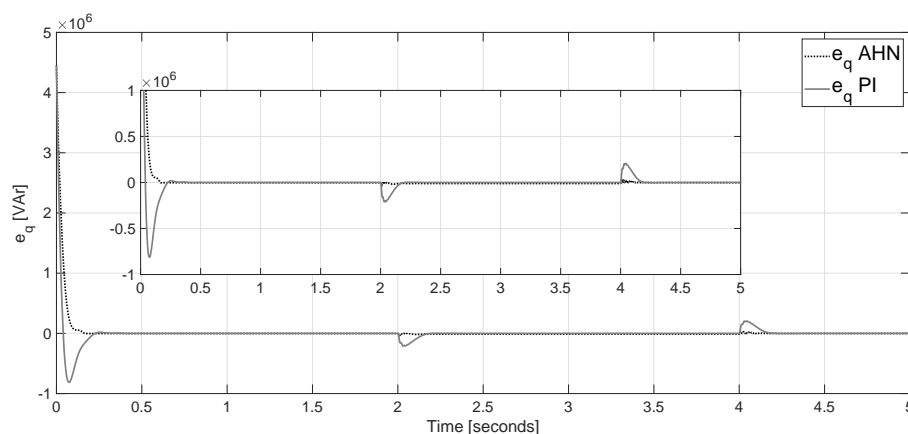
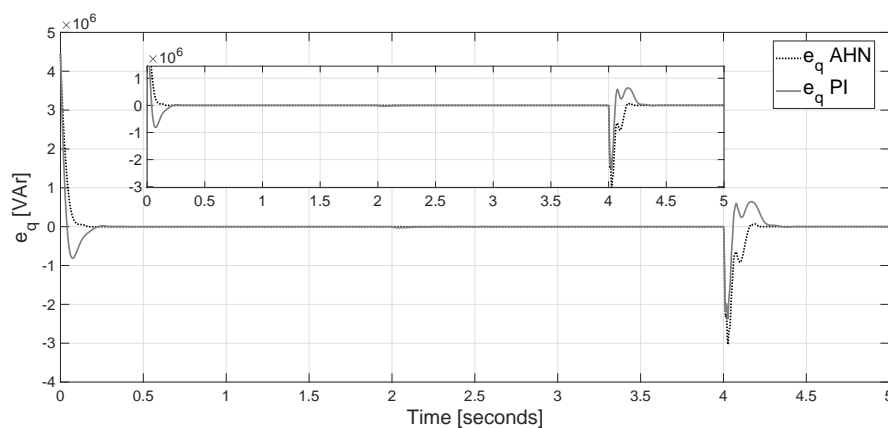


Figure 18. Simulation of the regulation error  $e_q$  of reactive power during Test 1.



**Figure 19.** Simulation of the regulation error  $e_q$  of reactive power during Test 2.



**Figure 20.** Simulation of the regulation error  $e_q$  of reactive power during Test 3.

Tables 2 and 3 present a comparison between the AHN controller and PI for Tests 1–3, with respect to regulation error and control effort, respectively. Table 2 considers the integral absolute error (IAE), computed as  $IAE = \int |e|dt$ , where  $e$  is the regulation error. The control energy presented in Table 3 is computed as  $Ctrl.Energy = \int |u|^2dt$ , where  $u$  is the control signal. It can be observed that the error of the AHN controller is similar than PI control. However, if the control effort in Table 3 is considered, the energy required by the PI control to reach a similar error to the AHN controller is at least two times larger.

**Table 2.** Comparison of Robust Scheme and PI: Error. IAE, integral absolute error.

Test	1	2	3
IAE [VAr], AHN	$1.86 \times 10^5$	$1.61 \times 10^5$	$3.22 \times 10^5$
IAE [VAr], PI	$1.61 \times 10^5$	$1.79 \times 10^5$	$3.16 \times 10^5$

**Table 3.** Comparison of Robust Scheme and PI: Control Effort.

Test	1	2	3
Ctrl. Energy, AHN	$3.51 \times 10^4$	$3.44 \times 10^4$	$3.16 \times 10^4$
Ctrl. Energy, PI	$5.13 \times 10^4$	$6.75 \times 10^4$	$9.93 \times 10^4$



## 6. Conclusions

The performance of distributed generators under unbalanced conditions can be improved considerably by replacing classical PID-type controllers by the proposed AHN controller. A smooth transient (minor overshoot) response in the reactive power regulation is obtained using the presented scheme based on AHN, compared with conventional controllers. Despite the quick response provided by the robust control proposal, the inertia is maintained by ensuring stability in the electric grid. Furthermore, the robustness of DG with an AHN controller can be observed, as the regulation of reactive power can be accomplished even in the presence of voltage sags and changes between connected and island modes (and vice versa), as is verified in the simulation results. The simulations results coincide with the theoretical conclusions about stability and robustness presented in the Lyapunov analysis.

**Author Contributions:** All the authors contributed equally to this work.

**Funding:** This research was funded by CONACYT (Consejo Nacional de Ciencia y Tecnología) SENER (Secretaría de Energía) Fund for Energy Sustainability (Agreement S0019201401).

**Acknowledgments:** This research is a product of the Project 266632 “Laboratorio Binacional para la Gestión Inteligente de la Sustentabilidad Energética y la Formación Tecnológica” (“Bi-National Laboratory on Smart Sustainable Energy Management and Technology Training”).

**Conflicts of Interest:** The authors declare no conflict of interest

## References

1. Agency, E.E. *Renewable Energy in Europe—2017 Update: Recent Growth and Knock-On Effects*; Technical Report 13; European Environment Agency: Copenhagen, Denmark, 2017. [\[CrossRef\]](#)
2. Board, N.E. *Canada’s Adoption of Renewable Power Sources: Energy Market Analysis*; Technical Report; National Energy Board: Calgary, AB, Canada, 2017.
3. Olivares, D.E.; Mehrizi-Sani, A.; Etemadi, A.H.; Cañizares, C.A.; Iravani, R.; Kazerani, M.; Hajimiragha, A.H.; Gomis-Bellmunt, O.; Saeedifard, M.; Palma-Behnke, R.; et al. Trends in Microgrid Control. *IEEE Trans. Smart Grid* **2014**, *5*, 1905–1919. [\[CrossRef\]](#)
4. Hirsch, A.; Parag, Y.; Guerrero, J. Microgrids: A review of technologies, key drivers, and outstanding issues. *Renew. Sustain. Energy Rev.* **2018**, *90*, 402–411. [\[CrossRef\]](#)
5. Schiffer, J.; Zonetti, D.; Ortega, R.; Stankovic, A.M.; Sezi, T.; Raisch, J. A survey on modeling of microgrids: From fundamental physics to phasors and voltage sources. *Automatica* **2016**, *74*, 135–150. [\[CrossRef\]](#)
6. Liu, J.; Miura, Y.; Ise, T. Comparison of Dynamic Characteristics Between Virtual Synchronous Generator and Droop Control in Inverter-Based Distributed Generators. *IEEE Trans. Power Electron.* **2016**, *31*, 3600–3611. [\[CrossRef\]](#)
7. Driesen, J.; Visscher, K. Virtual synchronous generators. In Proceedings of the 2008 IEEE Power and Energy Society General Meeting—Conversion and Delivery of Electrical Energy in the 21st Century, Pittsburgh, PA, USA, 20–24 July 2008; pp. 1–3. [\[CrossRef\]](#)
8. Bevrani, H.; Ise, T.; Miura, Y. Virtual synchronous generators: A survey and new perspectives. *Int. J. Electr. Power Energy Syst.* **2014**, *54*, 244–254. [\[CrossRef\]](#)
9. Shi, K.; Ye, H.; Xu, P.; Zhao, D.; Jiao, L. Low-voltage ride through control strategy of virtual synchronous generator based on the analysis of excitation state. *IET Gener. Transm. Distrib.* **2018**, *12*, 2165–2172. [\[CrossRef\]](#)
10. Shi, K.; Song, W.; Xu, P.; Liu, R.; Fang, Z.; Ji, Y. Low-Voltage Ride-Through Control Strategy for a Virtual Synchronous Generator Based on Smooth Switching. *IEEE Access* **2018**, *6*, 2703–2711. [\[CrossRef\]](#)
11. Zheng, T.; Chen, L.; Guo, Y.; Mei, S. Comprehensive control strategy of virtual synchronous generator under unbalanced voltage conditions. *IET Gener. Transm. Distrib.* **2018**, *12*, 1621–1630. [\[CrossRef\]](#)
12. Zheng, T.; Chen, L.; Guo, Y.; Mei, S. Flexible unbalanced control with peak current limitation for virtual synchronous generator under voltage sags. *J. Mod. Power Syst. Clean Energy* **2018**, *6*, 61–72. [\[CrossRef\]](#)
13. Rocabert, J.; Luna, A.; Blaabjerg, F.; Rodríguez, P. Control of Power Converters in AC Microgrids. *IEEE Trans. Power Electron.* **2012**, *27*, 4734–4749. [\[CrossRef\]](#)

14. Timbus, A.; Liserre, M.; Teodorescu, R.; Rodriguez, P.; Blaabjerg, F. Evaluation of Current Controllers for Distributed Power Generation Systems. *IEEE Trans. Power Electron.* **2009**, *24*, 654–664. [[CrossRef](#)]
15. Li, M.; Huang, W.; Tai, N.; Yu, M. Lyapunov-Based Large Signal Stability Assessment for VSG Controlled Inverter-Interfaced Distributed Generators. *Energies* **2018**, *11*, 2273. [[CrossRef](#)]
16. Pourroshanfekr, H.; Rokrok, E.; Javidsharifi, M. A robust back-stepping stabilization scheme for virtual synchronous generators in weak grids. In Proceedings of the 6th Power Electronics, Drive Systems Technologies Conference (PEDSTC2015), Tehran, Iran, 3–4 February 2015; pp. 509–514. [[CrossRef](#)]
17. Hu, Y.; Wei, W.; Peng, Y.; Lei, J. Fuzzy virtual inertia control for virtual synchronous generator. In Proceedings of the 2016 35th Chinese Control Conference (CCC), Chengdu, China, 27–29 July 2016; pp. 8523–8527. [[CrossRef](#)]
18. Tan, K.H.; Lan, C.W. DG System Using PFNN Controllers for Improving Islanding Detection and Power Control. *Energies* **2019**, *12*, 506. [[CrossRef](#)]
19. Wang, L.X. *A Course in Fuzzy Systems and Control*; Prentice-Hall, Inc.: Upper Saddle River, NJ, USA, 1997.
20. Ponce, H.; Ponce, P.; Molina, A. *Artificial Organic Networks: Artificial Intelligence Based on Carbon Networks*; Springer: Cham, Switzerland, 2014; Volume 521.
21. Ponce, H.; Ponce, P.; Molina, A. Artificial hydrocarbon networks fuzzy inference system. *Math. Probl. Eng.* **2013**, *2013*. [[CrossRef](#)]
22. Ponce, H.; Ponce, P.; Molina, A. Doubly fed induction generator (DFIG) wind turbine controlled by artificial organic networks. *Soft Comput.* **2017**, *22*, 2867–2879. [[CrossRef](#)]
23. Molina, A.; Ponce, H.; Ponce, P.; Tello, G.; Ramirez, M. Artificial hydrocarbon networks fuzzy inference systems for CNC machines position controller. *Int. J. Adv. Manuf. Technol.* **2014**, *9–12*, 1465–1479. [[CrossRef](#)]
24. Ponce, H.; Ponce, P.; Molina, A. A novel robust liquid level controller for coupled-tanks systems using artificial hydrocarbon networks. *Expert Syst. Appl.* **2015**, *22*, 8858–8867. [[CrossRef](#)]
25. Akagi, H.; Ogasawara, S.; Kim, H. The theory of instantaneous power in three-phase four-wire systems: A comprehensive approach. In Proceedings of the Thirty-Forth IAS Annual Meeting on Conference Record of the 1999 IEEE Industry Applications Conference, Phoenix, AZ, USA, 3–7 October 1999; Volume 1, pp. 431–439.
26. Hu, J.; Shang, L.; He, Y.; Zhu, Z.Q. Direct Active and Reactive Power Regulation of Grid-Connected DC/AC Converters Using Sliding Mode Control Approach. *IEEE Trans. Power Electron.* **2011**, *26*, 210–222. [[CrossRef](#)]
27. Kim, S.W.; Lee, J.J. Design of a fuzzy controller with fuzzy sliding surface. *Fuzzy Sets Syst.* **1995**, *71*, 359–367. [[CrossRef](#)]
28. Khalil, H. *Nonlinear Systems*; Prentice Hall: New Jersey, NJ, USA, 1996.
29. Ma, K.; Chen, W.; Liserre, M.; Blaabjerg, F. Power Controllability of a Three-Phase Converter with an Unbalanced AC Source. *IEEE Trans. Power Electron.* **2015**, *30*, 1591–1604. [[CrossRef](#)]



© 2019 by the authors. Licensee MDPI, Basel, Switzerland. This article is an open access article distributed under the terms and conditions of the Creative Commons Attribution (CC BY) license (<http://creativecommons.org/licenses/by/4.0/>).